Modeling and simulation of urban air pollution from the dispersion of vehicle exhaust: A continuum modeling approach

Liangze Yang[1], Tingting Li[2], S.C.Wong[3], Chi-Wang Shu[4] and Mengping Zhang[5]

Abstract

Air pollution has become a serious issue over the past few decades, and the transport sector is an important emission source. In this study, we model and simulate the dispersion of vehicle exhaust in a hypothetical city with a single central business district (CBD) in a complete day, deriving an average daily pollutant concentration, then use the distribution of wind direction over a year, to compute the distribution of average pollutant concentration in the city. All vehicles are assumed to be continuously distributed over the whole city, and the road network is relatively dense and can be approximated as a continuum. The model of Huang et al (2009, Transportation Research Part B, 43(1): 127-141) is used to describe the traffic flow that satisfies the reactive dynamic user equilibrium principle, and the pollution dispersion model is governed by the advection-diffusion equation. The complete model is composed of a coupled system of a conservation law, an eikonal equation and an advection-diffusion equation. The problem is solved by the efficient fifth-order weighted essentially non-oscillatory scheme for the conservation equation and the advection-diffusion equation, and the fast sweeping method for the eikonal equation with third order total variation diminishing (TVD) Runge-Kutta time

[1]School of Mathematical Sciences, University of Science and Technology of China, Hefei, Anhui 230026, P.R. China. E-mail: lzeyang@mail.ustc.edu.cn.

[2]School of Mathematics and Statistics, Henan University, Kaifeng, Henan 475001, P.R. China. E-mail: lttt1120@mail.ustc.edu.cn.

[3]Department of Civil Engineering, The University of Hong Kong, Pokfulam Road, Hong Kong, PR China. E-mail:hhecwsc@gmail.com.

[4]Division of Applied Mathematics, Brown University, Providence, RI 02912, USA. E-mail: shu@dam.brown.edu.

[5]School of Mathematical Sciences, University of Science and Technology of China, Hefei, Anhui 230026, P.R. China. E-mail: mpzhang@ustc.edu.cn.

discretization. The numerical results show a reasonable temporal and spatial distribution of vehicle density and pollution concentration.

Key Words: Advection-diffusion equation; Atmospheric dispersion; Continuum model.

1 Introduction

An air pollution dispersion model is often used to describe the contaminant transport in the atmosphere. The term dispersion describes the combination of diffusion (due to turbulent eddy motion) and advection (due to the wind) that occurs within the air near the Earth's surface. The concentration of a contaminant released into the air can be described by the advection-diffusion equation which is a second-order partial differential equation of the parabolic type.

Roberts (1923) and Sutton (1932) provided analytical and approximate solutions for the atmospheric dispersion problem in their pioneering studies, although some of their assumptions were over simplified. Many different dispersion models have been derived to address the various boundary conditions and parameter dependencies. The simplest of these models is the so-called Gaussian plume dispersion model (Stockie, 2011), corresponding to a continuous point source that emits contaminant into a uni-directional wind in an infinite domain. The Gaussian plume model began to attract more attention when Pasquill (1961) published his dispersion rates for plumes over open level terrain. The Gaussian plume model has achieved popularity because it is easy to use, the plume dispersion data are readily available, and most measured data fit the model reasonably well (Whaley, 1974).

Gaussian plume models have been applied extensively, and have numerous variants. They have been used to study emissions from multiple sources (Lushi and Stockie, 2010), such as air contaminant dispersion in a domain with an inversion layer (Wikipedia, 2010), and from line sources (Nagendra and Khare, 2002), area sources, instantaneous sources and time-varying sources (Arya, 1999). Ermak (1977) was the first to consider pollutant dispersion with both deposition and settling.

In this study we model and simulate the dispersion of pollution emitted from vehicles in a

hypothetical city with a single central business district (CBD) in a complete day, and consider dispersion under different wind directions. We also derive a distribution of an average pollutant concentration in a year within the city region. Our aim is to simulate the travel behavior of commuters to the CBD and back home. We adopt the continuum modeling approach which has been applied to the static analysis of air pollution pollutant in Yin et al. (2013, 2017). For this paper, we extended continuum modeling approach to the dynamic analysis of air pollution pollutant. We divide the problem into two parts. In the first, all vehicles leave their homes and travel to the CBD, with all vehicles eventually entering the CBD. In the second part, all vehicles leave the CBD and gradually go back to their homes, and eventually all vehicles have left the CBD and arrived at their homes. We use the model in Huang et al. (2009) to describe the traffic flow that satisfies the reactive dynamic user equilibrium principle in which a vehicle chooses a route to minimize the instantaneous travel cost to the destination. The dispersion emission model of Ahn et al. (1999) is then combined with the traffic model. The numerical results give the temporal and spatial distribution of the vehicle density and the pollution concentration within the modeling region.

2 Model formulation

As Figure 1 shows, the modeled region is an urban city denoted by Ω. Let Γ_o be the outer boundary of the city, Γ_c be the boundary of the compact CBD and Γ_i be the boundary of an obstruction such as a lake, park or undeveloped area where traffic is not allowed to enter. Thus, the boundary of Ω is $\Gamma = \Gamma_o \cup \Gamma_c \cup \Gamma_i$. The vehicles are continuously located within $(x, y) \in \Omega$, and they move back and forth to the CBD within the modeling region for a given time-dependent demand in a complete day.

We consider the dispersion of vehicle exhaust in a complete day in the city. For simplicity, we only consider the vehicles moving back and forth to the CBD from their homes, and ignore other travel behaviors. We divide the problem into two parts. In the first, all vehicles leave their homes and travel to the CBD, and there are no vehicles leaving the CBD, with the

travel demand being a non-negative function representing the vehicles joining the traffic system gradually. In the second part, all vehicles leave the CBD and travel back to their homes, and there are no vehicles traveling to the CBD, with the travel demand being a non-positive function representing the vehicles leaving the traffic system gradually.

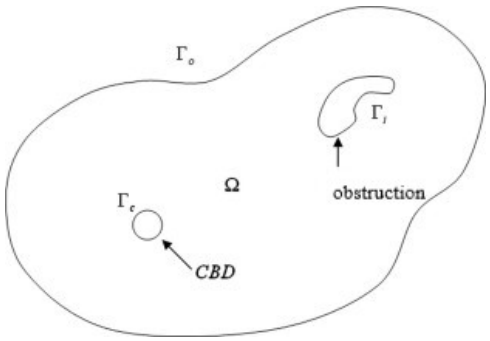

Fig. 1: The modeling domain

The variables are denoted as follows.

- $\rho(x, y, t)$ (in veh/km^2) is the density of travelers at the location (x, y) and at time t.
- $\boldsymbol{v} = (u(x, y, t), v(x, y, t))$ is the velocity vector at the location (x, y) and at time t.
- $U(x, y, t)$ (in km/h) is the speed, which is the norm of the velocity vector, i.e., $U = |\boldsymbol{v}|$, and is determined by the density as

$$U(x, y, t) = U_f e^{-\beta\rho^2}, \quad \forall (x, y) \in \Omega, \ t \in T^j. \tag{1}$$

  where $U_f(x, y)$ (in km/h) is the free-flow speed and $\beta(x, y)$ (in km^4/veh^2) is a positive scalar related to the road condition.

- $\boldsymbol{F} = (f_1(x, y, t), f_2(x, y, t))$ is the flow vector at the location (x, y) and at time t, which is defined as

$$\boldsymbol{F} = \rho\boldsymbol{v}, \quad \forall (x, y) \in \Omega, \ \ t \in T^j. \tag{2}$$

- $|\boldsymbol{F}|$ is the flow intensity, which is the norm of the flow vector $\boldsymbol{F}$, and is defined as

$$|\boldsymbol{F}| = \rho U, \quad \forall (x, y) \in \Omega, \ \ t \in T^j. \tag{3}$$

- $q(x, y, t)$ (in $veh/km^2/h$) is the travel demand at the location (x, y) and at time t, which is a time-varying function.

- $c(x, y, t)$ (in $\$/km$) is the local travel cost per unit distance of travel at the location (x, y) and at time t, and is defined as

$$c(x, y, t) = \kappa(\frac{1}{U} + \pi(\rho)), \quad \forall (x, y) \in \Omega, \ \ t \in T^j. \tag{4}$$

  where κ is the value of time, $\frac{\kappa}{U}$ represents the cost associated with the travel time, and $\kappa\pi(\rho)$ represents other costs that are dependent on the density.

- $\phi(x, y, t)$ is the instantaneous travel cost potential of the traveler who departs from the location (x, y) at time t to travel to the CBD using the constructed path-choice strategy.

- $\phi_1(x, y, t)$ is the instantaneous travel cost potential of the traveler who departs from the CBD travel to the location (x, y) at time t using the constructed path-choice strategy.

- $C(x, y, z, t)$ (in kg/km^3) is the concentration of the pollution at the location (x, y, z) and at time t.

- $\boldsymbol{u_f}(x, y, z, t)$ (in km/h) is the wind velocity vector at the location (x, y, z) and at time t.

- K_x, K_y, K_z (in km^2/h) are the eddy diffusivities in the x, y and z directions, respectively.

- E (in $kg/(veh\ h)$) is the amount of pollutant generated per vehicle and per hour.

Finally, $T = T^1 \cup T^2$, for $j \in \{1, 2\}$, $T^j = [t^j_{beginning}, t^j_{end}]$ is the modeling period of the j-th part of the traffic. T^1 refers to the traffic period going to the CBD, and T^2 refers to the traffic period coming back home from the CBD.

2.1 The traffic model formulation of vehicles traveling to the CBD

In this part, all vehicles travel to the CBD. Similar to flow conservation in fluid dynamics, the traffic density, flow vector, and demand are governed by the flow conservation equation:

$$\rho_t(x, y, t) + \nabla \cdot \boldsymbol{F}(x, y, t) = q(x, y, t), \quad \forall (x, y) \in \Omega, \ \ t \in T^1. \tag{5}$$

where $\rho_t(x,y,t) = \frac{\partial \rho(x,y,t)}{\partial t}$, and $\nabla \cdot \boldsymbol{F}(x,y,t) = \frac{\partial f_1(x,y,t)}{\partial x} + \frac{\partial f_2(x,y,t)}{\partial y}$.

To ensure that vehicles from a given location $(x,y) \in \Omega$ will choose a path that minimizes their individual traveling cost to the destination, based on the instantaneous travel cost information that is available at the time of decision making (Huang et al., 2009), we require that

$$c(x,y,t)\frac{\boldsymbol{F}(x,y,t)}{|\boldsymbol{F}(x,y,t)|} + \nabla\phi(x,y,t) = 0. \tag{6}$$

From Eq. (6), we can observe the following property

$$\boldsymbol{F}(x,y,t)// - \nabla\phi(x,y,t). \tag{7}$$

where // indicates that the two vectors are parallel and point in the same direction. In other words, the vector of the flux points in the opposite direction of the gradient to the cost potential. In addition, we have

$$\| \nabla\phi(x,y,t) \| = c(x,y,t), \quad \forall (x,y) \in \Omega, \ \ t \in T^1. \tag{8}$$

which is an eikonal equation.

The system is subject to the following initial and boundary conditions

$$\begin{cases} \boldsymbol{F}(x,y,t) \cdot \boldsymbol{n}(x,y) = 0, & \forall (x,y) \in \Gamma_o \cup \Gamma_i, \ t \in T^1, \\ \rho(x,y,t^1_{beginning}) = \rho_0(x,y), & \forall (x,y) \in \Omega, \\ \phi(x,y,t) = \phi_{CBD}, & \forall (x,y) \in \Gamma_c, \ t \in T^1. \end{cases} \tag{9}$$

where $\boldsymbol{n}(x,y)$ is the outward unit normal vector of the boundary, $\rho_0(x,y)$ is the density of traffic at location (x,y) at the beginning of the modeling period, and ϕ_{CBD} is the cost to the traveler of crossing the CBD.

2.2 The model formulation of vehicles returning from the CBD

In this subsection, we consider the vehicles returning to their homes from the CBD. The traffic flow on the boundary Γ_c is unknown and the destinations of different vehicles leaving Γ_c are different, so we cannot use the traffic model from the previous section of vehicles traveling into the CBD directly. In this paper, when considering the vehicle returning from the CBD,

we assume that this problem is just a reversed problem of the vehicle traveling to the CBD, i.e. if there are m vehicles reaching their home at time t, in contrast, backward in time, there are m vehicles leaving their home traveling to the CBD at time t. We should note that, because we give the rule of the vehicle reaching their home in the second modeling period, in other word, the travel demand function q is known, the inflow boundary condition of ρ at the CBD of the second modeling period should be a fixed function such that each traveler can return home at the time specified by the source term, and we can obtain it after the whole problem is solved. The travel demand can ensure that all vehicles have left the CBD and reached their home at the end of the modeling period. Next we establish the complete model formulation of the problem.

The conservation law equation still holds, with the flux satisfying

$$\boldsymbol{F} = \rho \boldsymbol{v} = \rho U \frac{\nabla \phi_1}{|\nabla \phi_1|}. \tag{10}$$

where the potential function ϕ_1 in the reactive dynamic user equilibrium can still be solved by eikonal equation.

For any used path p from the location $(x, y) \in \Omega$ to home $(x_0, y_0) \in \Omega$, if we integrate the local traveling cost along the path, then the total cost incurred by the vehicles can be obtained as

$$\begin{aligned} \Pi_p(x, y, t) &= \int_p c(x, y, t) ds = \int_p c(x, y, t) \frac{\boldsymbol{F}(x, y, t)}{\| \boldsymbol{F}(x, y, t) \|} \cdot \boldsymbol{ds}, \\ &= \int_p \nabla \phi_1(x, y, t) \cdot \boldsymbol{ds} = \phi_1(x_0, y_0, t) - \phi_1(x, y, t). \end{aligned} \tag{11}$$

using the above equations and given that $\frac{\boldsymbol{F}(x,y,t)}{\|\boldsymbol{F}(x,y,t)\|}$ is a unit vector parallel to $\boldsymbol{ds}$ along the path. Hence, the total instantaneous travel cost at time $t \in T^2$ is independent of the used paths.

In contrast, for any unused path $\tilde{p}$ between a location $(x, y) \in \Omega$ to home $(x_0, y_0) \in \Omega$, the total cost incurred by the vehicles is

$$\begin{aligned} \Pi_{\tilde{p}}(x, y, t) &= \int_{\tilde{p}} c(x, y, t) ds \geq \int_{\tilde{p}} c(x, y, t) \frac{\boldsymbol{F}(x, y, t)}{\| \boldsymbol{F}(x, y, t) \|} \cdot \boldsymbol{ds}, \\ &= \int_{\tilde{p}} \nabla \phi_1(x, y, t) \cdot \boldsymbol{ds} = \phi_1(x_0, y_0, t) - \phi_1(x, y, t). \end{aligned} \tag{12}$$

The inequality in the above derivation occurs because for some segments along the path $\tilde{p}$, the normal vector $\frac{\boldsymbol{F}(x,y,t)}{\|\boldsymbol{F}(x,y,t)\|}$ and $\boldsymbol{ds}$ may not be parallel, and thus $ds \geq \frac{\boldsymbol{F}}{\|\boldsymbol{F}\|} \cdot \boldsymbol{ds}$ for those segments. Hence, for any unused paths, the total instantaneous cost is greater than or equal to that of the used paths. The model thus guarantees that vehicles will choose their paths in a user-optimal manner with respect to the instantaneous travel information.

The system is subject to the following initial and boundary conditions

$$\begin{cases} \boldsymbol{F}(x,y,t) \cdot \boldsymbol{n}(x,y) = 0, & \forall (x,y) \in \Gamma_o \cup \Gamma_i,\ t \in T^2, \\ \rho(x,y,t^2_{end}) = 0, & \forall (x,y) \in \Omega, \\ \phi_1(x,y,t) = \phi_{CBD}, & \forall (x,y) \in \Gamma_c,\ t \in T^2. \end{cases} \tag{13}$$

Note that the "initial" condition is given at the ending time $t = t^2_{end}$ in the traffic model. When shocks appear and the solution is not reversible, this "backward solving" of the conservation law is not well defined. However, if we consider only continuous solutions without shocks (as we do in this study), the solution is reversible, and if we define:

$$\begin{gathered} \tau = t^2_{end} - t + t^2_{beginning},\ \ \tilde{\rho}(x,y,\tau) = \rho(x,y,t^2_{end} - \tau),\ \ \tilde{q}(x,y,\tau) = -q(x,y,t^2_{end} - \tau), \\ \tilde{\boldsymbol{F}}(x,y,\tau) = -\boldsymbol{F}(x,y,t^2_{end} - \tau),\ \ \tilde{\phi}(x,y,\tau) = \phi_1(x,y,t^2_{end} - \tau),\ \ \tilde{c}(x,y,\tau) = c(x,y,t^2_{end} - \tau). \end{gathered} \tag{14}$$

then we can rewrite the time-dependent equation into the standard form:

$$\begin{cases} \tilde{\rho}_\tau + \nabla \cdot \tilde{\boldsymbol{F}}(x,y,\tau) = \tilde{q}(x,y,\tau), & \forall (x,y) \in \Omega,\ \ \tau \in \tilde{T}^2, \\ \parallel \nabla \tilde{\phi}(x,y,\tau) \parallel = \tilde{c}(x,y,\tau), & \forall (x,y) \in \Omega,\ \ \tau \in \tilde{T}^2, \\ \tilde{\boldsymbol{F}} = \tilde{\rho}\boldsymbol{v} = \tilde{\rho} U \dfrac{-\nabla \tilde{\phi}(x,y,\tau)}{\parallel \nabla \tilde{\phi}(x,y,\tau) \parallel}, & \forall (x,y) \in \Omega,\ \ \tau \in \tilde{T}^2. \end{cases} \tag{15}$$

where $\tilde{T^2}$ is the image of T^2 under the transformation from t to τ. Therefore, the problem of vehicles returning from the CBD is simply a reversed problem of the vehicles traveling to the CBD.

2.3 Advection-diffusion equation

In this subsection, we consider the dispersion of vehicle exhaust due to the turbulent diffusion and advection of the wind. The concentration $C(x,y,z,t)$ is governed by the following

three-dimensional advection-diffusion equation

$$\frac{\partial C}{\partial t} + \nabla \cdot (C\boldsymbol{u_f}) = \frac{\partial}{\partial x}(K_x \frac{\partial C}{\partial x}) + \frac{\partial}{\partial y}(K_y \frac{\partial C}{\partial y}) + \frac{\partial}{\partial z}(K_z \frac{\partial C}{\partial z}) + S. \tag{16}$$

where $S(x, y, z, t)$ $[kg/(km^3\ h)]$ is a source term. We next make several simplifying assumptions:

- Variations in topography are negligible so the ground surface can be taken as the plane $z = 0$.
- The contaminant is emitted at the rate $Q = \rho E$ $[kg/(km^2\ h)]$ from a surface source at $z = 0$, and E will be discussed in the next section. Then the source term can be written as

$$S(x, y, z, t) = Q\delta(z). \tag{17}$$

  where $\delta(\cdot)$ is the Dirac delta function. Note that the unit of the delta function is km^{-1}.
- The wind velocity is constant so that $\boldsymbol{u_f} = (u_f, v_f, w_f)$ for the constants u_f, v_f, w_f. For simplicity and without loss of generality, we assume that the wind direction is along the positive x direction, that is, $u_f > 0$, $v_f = w_f = 0$.
- The diffusion is isotropic so the eddy diffusivities satisfy $K_x = K_y = K_z = K$.
- The wind velocity is sufficiently large, so the diffusion in the x-direction is much lower than the advection, and thus the term $K_x \partial_x^2 C$ can be neglected.

Under these assumptions, the equation (16) reduces to

$$\frac{\partial C}{\partial t} + \frac{\partial (u_f C)}{\partial x} = \frac{\partial}{\partial y}(K \frac{\partial C}{\partial y}) + \frac{\partial}{\partial z}(K \frac{\partial C}{\partial z}) + \rho E \delta(z). \tag{18}$$

As the uni-directional wind and the assumption that there are no vehicles for $x < 0$, and as the contaminant does not penetrate the ground, we have the boundary conditions

$$C(0, y, z, t) = 0, \quad K \frac{\partial C}{\partial z}(x, y, 0, t) = 0. \tag{19}$$

2.4 The emission model

Several models can estimate transport-related pollutant emissions. Here, the acceleration and speed-based model is used, in which the emission rate is defined as a function of vehicle type, instantaneous speed, and acceleration. We apply the model proposed by Ahn et al. (1999), in which the emission rate is defined as a function of the instantaneous acceleration and speed as follows:

$$E = \exp(\sum_{i=0}^{3}\sum_{j=0}^{3} w_{i,j} U^i a^j). \tag{20}$$

where a is the instantaneous acceleration (km/h^2), U is the instantaneous speed (km/h), $w_{i,j}$ is the model regression coefficient for speed power i and acceleration power j, and the coefficient may be different according to different kinds of emissions such as HC, CO, and NO_x (mg/s).

There is no single representative measure of traffic related air pollution. However, as suggested by Wardman and Bristow (2004), NO_x levels can be usefully selected, as this pollutant has clearly adverse health effects. Here, we consider only the NO_x emissions. The parameters (Ahn et al., 1999) involved are summarized in Table 1.

Under the route choice governed by user-optimal conditions, vehicles may accelerate or decelerate along their trajectory, according to the spatial variation in traffic conditions in the neighboring area. The acceleration in the direction of movement is determined by

$$a = \frac{a_x \phi_x + a_y \phi_y}{\sqrt{(\phi_x^2 + \phi_y^2)}}. \tag{21}$$

where a_x, a_y represent accelerations in the x and y directions, respectively, and the following equations should be satisfied:

$$a_x = u_t + uu_x + vu_y, \quad a_y = v_t + uv_x + vv_y. \tag{22}$$

Table 1: Parameters for estimating NO_x emissions

i,j	0	1	2	3
0	-1.07E+00	6.44E-05	5.68E-10	-1.54E-14
1	4.23E-02	3.57E-06	1.68E-10	-4.73E-15
2	-1.41E-04	-2.73E-08	-3.14E-12	2.61E-17
3	4.31E-07	6.28E-11	1.16E-14	-1.60E-19

2.5 The complete model

After the previous discussion, we can write our model for the two parts.

The complete model of the vehicles traveling to the CBD:

$$\begin{cases} \rho_t + \nabla \cdot \boldsymbol{F}(x,y,t) = q(x,y,t), & \forall (x,y) \in \Omega, \ \ t \in T^1, \\ \| \nabla \phi(x,y,t) \| = c(x,y,t), & \forall (x,y) \in \Omega, \ \ t \in T^1, \\ \boldsymbol{F} = \rho \boldsymbol{v} = \rho U \dfrac{(-\nabla \phi(x,y,t))}{\| \nabla \phi(x,y,t) \|}, & \forall (x,y) \in \Omega, \ \ t \in T^1, \\ \dfrac{\partial C}{\partial t} + \dfrac{\partial (u_f C)}{\partial x} = \dfrac{\partial}{\partial y}(K \dfrac{\partial C}{\partial y}) + \dfrac{\partial}{\partial z}(K \dfrac{\partial C}{\partial z}) + \rho E \delta(z), & \forall (x,y,z) \in \bar{\Omega}, \ t \in T^1. \end{cases} \tag{23}$$

The system (23) is subject to the following initial and boundary conditions:

$$\begin{cases} \boldsymbol{F}(x,y,t) \cdot \boldsymbol{n}(x,y) = 0, & \forall (x,y) \in \Gamma_0 \cup \Gamma_i, \ t \in T^1, \\ \rho(x,y,t^1_{beginning}) = 0, & \forall (x,y) \in \Omega, \\ \phi(x,y,t) = 0, & \forall (x,y) \in \Gamma_c, \ t \in T^1, \\ C(0,y,z,t) = 0, \ \ K \dfrac{\partial C}{\partial z}(x,y,0,t) = 0, & (x,y,z) \in \bar{\Omega}, \ t \in T^1, \\ C(x,y,z,0) = 0, & \forall (x,y,z) \in \bar{\Omega}. \end{cases} \tag{24}$$

The complete model of the vehicles returning from the CBD:

$$\begin{cases} \rho_t + \nabla \cdot \boldsymbol{F}(x,y,t) = q(x,y,t), & \forall (x,y) \in \Omega, \ \ t \in T^2, \\ \| \nabla \phi_1(x,y,t) \| = c(x,y,t), & \forall (x,y) \in \Omega, \ \ t \in T^2, \\ \boldsymbol{F} = \rho \boldsymbol{v} = \rho U \dfrac{(\nabla \phi_1(x,y,t))}{\| \nabla \phi_1(x,y,t) \|}, & \forall (x,y) \in \Omega, \ \ t \in T^2, \\ \dfrac{\partial C}{\partial t} + \dfrac{\partial (u_f C)}{\partial x} = \dfrac{\partial}{\partial y}(K \dfrac{\partial C}{\partial y}) + \dfrac{\partial}{\partial z}(K \dfrac{\partial C}{\partial z}) + \rho E \delta(z), & \forall (x,y,z) \in \bar{\Omega}, \ t \in T^2. \end{cases} \tag{25}$$

The system (25) is subject to the following initial and boundary conditions:

$$\begin{cases} \boldsymbol{F}(x,y,t)\cdot\boldsymbol{n}(x,y)=0, & \forall (x,y)\in\Gamma_0\cup\Gamma_i,\ t\in T^2,\\ \rho(x,y,t_{end}^2)=0, & \forall (x,y)\in\Omega,\\ \phi_1(x,y,t)=0, & \forall (x,y)\in\Gamma_c,\ t\in T^2,\\ C(0,y,z,t)=0,\ \ K_z\dfrac{\partial C}{\partial z}(x,y,0,t)=0, & (x,y,z)\in\bar{\Omega},\ t\in T^2\\ C(x,y,z,t_{beginning}^2)=C_0(x,y,z), & \forall (x,y,z)\in\bar{\Omega}. \end{cases} \tag{26}$$

Here, $\bar{\Omega}$ is the dispersion region, $C_0(x,y,z)$ is the concentration of pollution at location (x,y) at the beginning of the second part, which equals to the value of concentration at the end of the first part. $\rho(x,y,t)$ is governed by the conservation law, $\phi(x,y,t)$, $\phi_1(x,y,t)$ is computed by using the eikonal equation, and $C(x,y,z,t)$ is governed by the advection-diffusion equation. Note that, when we solve the second model by using a transformation $\tau = t_{end}^2 - t + t_{beginning}^2$, the initial time in the conservation law is set at $\tau = t_{beginning}^2$, and the solution of the advection-diffusion equation is still solved in the original t variable with the initial condition at $t = t_{beginning}^2$.

3 The solution algorithm

In this section, we describe an efficient solution method for solving the whole model. The fifth order weighted essentially non-oscillatory (WENO) scheme is used for the conservation law equation. The fast sweeping method based on the third WENO scheme is used for the eikonal equation. For solving the advection-diffusion equation, the first order spatial derivative is approximated by the fifth order WENO method, and the second order spatial derivatives are approximated by the fourth order central discretization. Finally, the third order total-variation-diminishing (TVD) Runge-Kutta time discretization is used to solve the coupled system of equations in time.

3.1 The fifth-order WENO scheme for the conservation law

For the 2D mass conservation equation of the system, the semi-discrete scheme approximates the point values $\rho_{i,j} \approx \rho(x_i, y_j, t)$ through a conservative difference formula as follows

$$\frac{d}{dt}\rho_{i,j} = -\frac{1}{\Delta x}((\hat{f}_1)_{i+\frac{1}{2},j} - (\hat{f}_1)_{i-\frac{1}{2},j}) - \frac{1}{\Delta y}((\hat{f}_2)_{i,j+\frac{1}{2}} - (\hat{f}_2)_{i,j-\frac{1}{2}}) + q_{i,j}\Delta t. \tag{27}$$

where $q_{i,j} = q(x_i, y_j, t)$ is the given demand at the location (x_i, y_j) and at time t, Δx and Δy are the mesh sizes in x and y, respectively, which are assumed to be uniform $\Delta x = \Delta y = h$ for simplicity. $(\hat{f}_1)_{i+\frac{1}{2},j}$ and $(\hat{f}_2)_{i,j+\frac{1}{2}}$ are the numerical fluxes in the x and y directions, respectively. We give details of the definition of the x-flux $(\hat{f}_1)_{i+\frac{1}{2},j}$ below. The definition for the y-flux $(\hat{f}_2)_{i,j+\frac{1}{2}}$ is analogous. When computing the x-flux $(\hat{f}_1)_{i+\frac{1}{2},j}$, the y index j is fixed. Therefore, for simplicity of notations, we drop the y index j below when there is no confusion.

We briefly summarize the high-order WENO schemes (Liu et al., 1994; Jiang and Shu, 1996; Shu, 1998) in this subsection. WENO schemes are popular for simulating problems with discontinuous or sharp varying solutions, and are used widely in many applications, such as in computational dynamics (CFD) and in traffic flow modeling. The basic idea of the WENO scheme is a locally adaptive choice of the approximation stencil, so that high-order accuracy is achieved in smooth regions and discontinuities are resolved in a sharp and non-oscillatory fashion. We use the fifth order finite difference WENO scheme in Jiang and Shu (1996) to approximate the numerical flux $(\hat{f}_1)_{i+\frac{1}{2}}$ in Eq. (27). We first assume $f_1'(\rho) \geq 0$, namely, a positive wind direction, to simplify the description. We will comment on the general case later. Here, the numerical flux $(\hat{f}_1)_{i+\frac{1}{2},j}$ is obtained through a one-point upwind-biased stencil containing $s_\ell = f_1(x_\ell, y_j, t)$ for $\ell = i-2, i-1, ..., i+2$. First, we form the following third-order numerical fluxes based on three different sub-stencils given by

$$\begin{aligned}
\hat{s}^{(1)}_{i+\frac{1}{2}} &= \frac{1}{3}s_{i-2} - \frac{7}{6}s_{i-1} + \frac{11}{6}s_i, \\
\hat{s}^{(2)}_{i+\frac{1}{2}} &= -\frac{1}{6}s_{i-1} + \frac{5}{6}s_i + \frac{1}{3}s_{i+1}, \\
\hat{s}^{(3)}_{i+\frac{1}{2}} &= \frac{1}{3}s_i + \frac{5}{6}s_{i+1} - \frac{1}{6}s_{i+2}.
\end{aligned} \tag{28}$$

We then define the three nonlinear weights ω_r for $r = 1, 2, 3$, by

$$\omega_r = \frac{\alpha_r}{\sum_{s=1}^{3} \alpha_s}, \quad \alpha_r = \frac{d_r}{(\varepsilon + \beta_r)^2}. \tag{29}$$

where the linear weights d_r are given by

$$d_1 = \frac{1}{10}, \;\; d_2 = \frac{3}{5}, \;\; d_3 = \frac{3}{10}. \tag{30}$$

and the smoothness indicators β_r, which measure the smoothness of the approximation in the r-th sub-stencil, are given by

$$\begin{aligned}
\beta_1 &= \frac{13}{12}(s_{i-2} - 2s_{i-1} + s_i)^2 + \frac{1}{4}(s_{i-2} - 4s_{i-1} + 3s_i)^2, \\
\beta_2 &= \frac{13}{12}(s_{i-1} - 2s_i + s_{i+1})^2 + \frac{1}{4}(s_{i-1} - s_{i+1})^2, \\
\beta_3 &= \frac{13}{12}(s_i - 2s_{i+1} + s_{i+2})^2 + \frac{1}{4}(s_i - 4s_{i+1} + 3s_{i+2})^2.
\end{aligned} \tag{31}$$

Here, ε is a parameter to prevent the denominator from becoming 0, and is taken as 10^{-6} in our computation. Finally,the numerical flux $(\hat{f}_1)_{i+\frac{1}{2},j}$ is given by the following convex combination of the three third-order fluxes as

$$(\hat{f}_1)_{i+\frac{1}{2},j} = \omega_1 s^{(1)}_{i+\frac{1}{2}} + \omega_2 s^{(2)}_{i+\frac{1}{2}} + \omega_3 s^{(3)}_{i+\frac{1}{2}}. \tag{32}$$

with the nonlinear weights given by (29).

For the general case where $f_1^{'}(\rho)$ may change sign, first we form a flux splitting $f_1(\rho) = f_1^{+}(\rho) + f_1^{-}(\rho)$ so that $\frac{d}{d\rho} f_1^{+}(\rho) \geq 0$ and $\frac{d}{d\rho} f_1^{-}(\rho) \leq 0$. We then perform the procedure above to obtain the numerical flux corresponding to $f_1^{+}(\rho)$, and use a mirror symmetric procedure, with respect to the location $x_{i+\frac{1}{2}}$, to obtain the numerical flux corresponding to $f_1^{-}(\rho)$. These two numerical fluxes are then combined to form the final numerical flux. Several flux splittings are used in practice, the most common being the Lax-Friedrichs splitting, which is given by

$$f_1^{\pm}(\rho) = \frac{1}{2}(f_1(\rho) \pm \alpha\rho), \;\; \text{where } \alpha = \max |f_1^{'}(\rho)|. \tag{33}$$

However, in our model, $f_1(\rho)$ is not an explicit function of ρ (see the definition of $\boldsymbol{F}$ in (10)). If we assume the velocity U and the potential ϕ are independent on ρ, then we have $f_1^{'}(\rho) =$

$U\frac{\phi_x}{\|\nabla\phi\|}$, and

$$\alpha = \max_i |(U\frac{\phi_x}{\| \nabla\phi \|})_i|. \tag{34}$$

3.2 The fast sweeping method for the eikonal equation

The eikonal equation is a special type of steady-state Hamilton-Jacobi equations. Solutions to Hamilton-Jacobi equations are usually continuous but not differentiable everywhere and are usually not unique. The viscosity solution Crandall and Lions (1983) is the physically relevant solution and the numerical solution for approximating the viscosity solutions of the Hamilton-Jacobi equations follows the lines similar to those for solving conservation laws. Thus the WENO schemes for conservation laws are extended to those for Hamilton-Jacobi equations in (Jiang and Peng, 2000; Shu, 2007). For the steady-state equation, if we use the time-dependent WENO scheme of (Jiang and Peng, 2000; Shu, 2007), we would need to introduce a pseudo-time and then march to a steady state. The fast sweeping method (Zhang et al., 2006) is much faster in terms of computational time than pseudo-time marching. We use the fast sweeping method to solve the eikonal equation (8) here. The first and third order fast sweeping methods can be found in (Zhao, 2005; Zhang et al., 2006; Xiong et al., 2011).

The fast sweeping method starts with the following initialization. Based on the boundary condition $\phi(x, y) = \phi_{CBD}$ for $(x, y) \in \Gamma_c$, we assign the exact boundary values on Γ_c. For the first order fast sweeping method, large values (for example 10^{12}) are assigned as the initial guess at all other grid points. For the third-order fast sweeping method, the solution from the first-order fast sweeping method is used as the initial guess at all other grid points.

The following Gauss-Seidel iterations with four alternating direction sweepings are performed after initialization

$$\begin{aligned} &(1)\ \ i = 1 : N_x,\ \ j = 1 : N_y; \qquad (2)\ \ i = N_x : 1,\ \ j = 1 : N_y; \\ &(3)\ \ i = N_x : 1,\ \ j = N_y : 1; \qquad (4)\ \ i = 1 : N_x,\ \ j = N_y : 1. \end{aligned} \tag{35}$$

where (i, j) is the grid index pair in (x, y) and N_x and N_y are the number of grid points in x and y, respectively. When we loop to a point (i, j), the solution is updated as follows, using the

Godunov Hamiltonian

$$\phi_{i,j}^{new} = \begin{cases} \min(\phi_{i,j}^{xmin}, \phi_{i,j}^{ymin}) + c_{i,j}h, & \text{if } |\phi_{i,j}^{xmin} - \phi_{i,j}^{ymin}| \le c_{i,j}h, \\ \dfrac{\phi_{i,j}^{xmin} + \phi_{i,j}^{ymin} + (2c_{i,j}^2h^2 - (\phi_{i,j}^{xmin} - \phi_{i,j}^{ymin})^2)^{\frac{1}{2}}}{2}, & \text{otherwise.} \end{cases} \tag{36}$$

where $c_{i,j} = c(x_i, y_j, t)$.

For a first-order fast sweeping method, we define $\phi_{i,j}^{xmin}$ and $\phi_{i,j}^{ymin}$ as

$$\begin{cases} \phi_{i,j}^{xmin} = \min(\phi_{i-1,j}, \phi_{i+1,j}), \\ \phi_{i,j}^{ymin} = \min(\phi_{i,j-1}, \phi_{i,j+1}). \end{cases} \tag{37}$$

For a third-order fast sweeping method, we define $\phi_{i,j}^{xmin}$ and $\phi_{i,j}^{ymin}$ as

$$\begin{cases} \phi_{i,j}^{xmin} = \min(\phi_{i,j}^{old} - h(\phi_x)_{i,j}^{-}, \phi_{i,j}^{old} + h(\phi_x)_{i,j}^{+}), \\ \phi_{i,j}^{ymin} = \min(\phi_{i,j}^{old} - h(\phi_y)_{i,j}^{-}, \phi_{i,j}^{old} + h(\phi_y)_{i,j}^{+}). \end{cases} \tag{38}$$

with

$$(\phi_x)_{i,j}^{-} = (1 - \omega_-)(\frac{\phi_{i+1,j} - \phi_{i-1,j}}{2h}) + \omega_-(\frac{3\phi_{i,j} - 4\phi_{i-1,j} + \phi_{i-2}}{2h}). \tag{39}$$

$$(\phi_x)_{i,j}^{+} = (1 - \omega_+)(\frac{\phi_{i+1,j} - \phi_{i-1,j}}{2h}) + \omega_+(\frac{-3\phi_{i,j} + 4\phi_{i+1,j} - \phi_{i+2}}{2h}). \tag{40}$$

$$\omega_- = \frac{1}{1 + 2r_-^2}, \qquad r_- = \frac{\varepsilon + (\phi_{i,j} - 2\phi_{i-1,j} + \phi_{i-2,j})^2}{\varepsilon + (\phi_{i+1,j} - 2\phi_{i,j} + \phi_{i-1,j})^2}. \tag{41}$$

$$\omega_+ = \frac{1}{1 + 2r_+^2}, \qquad r_+ = \frac{\varepsilon + (\phi_{i,j} - 2\phi_{i+1,j} + \phi_{i+2,j})^2}{\varepsilon + (\phi_{i+1,j} - 2\phi_{i,j} + \phi_{i-1,j})^2}. \tag{42}$$

where the nonlinear weights are the same as the third-order WENO schemes, and as the meaning of ε, except they are written in a different form as in (Jiang and Peng, 2000).

Convergence is declared if

$$\|\phi^{new} - \phi^{old}\| \le \delta. \tag{43}$$

where δ is a given convergence threshold value. $\delta = 10^{-9}$ and L^1 norm are used in our computation.

For the third-order fast sweeping method, using the nonlinear weights may cause non-convergence in some time steps for solving the system but the iteration does converge if linear weights are used instead. In order to avoid oscillatory results, particularly around the boundary where discontinuities exist, we use the strategy introduced in (Xiong et al., 2011). Firstly, we use the nonlinear weights to iterate. After the iteration error stagnates for 50 consecutive steps at the same error level, for example at 10^{-8}, we switch to fixed values for the weights taken as the average values of the nonlinear weights in those 50 iteration steps. These fixed weights are then used in (39) and (40) instead of the nonlinear weights (41) and (42) afterwards, which leads to very fast convergence according to (43).

3.3 Schemes for the advection-diffusion equation

In this subsection, we focus on the numerical method to solve the advection-diffusion equation with the Dirac source term. For the first order derivative, we use the fifth-order finite difference WENO scheme previously described, and the fourth-order standard central finite difference to approximate the second derivatives.

The Dirac function is a singular term in the differential equation, which is difficult to approximate in numerical computation. Based on the finite difference method, the most common and effective technique is to find a more regular function to approximate the Dirac function, the detailed description of which can be found in Tornberg and Engquist (2004). Here we use the following approximation to replace the Dirac function:

$$\delta_\varepsilon(z) = \begin{cases} \dfrac{1}{4\Delta z}\min(\dfrac{z}{\Delta z}+2, 2-\dfrac{z}{\Delta z}), & |z| \le 2\Delta z, \\ 0, & |z| > 2\Delta z. \end{cases} \tag{44}$$

3.4 The third-order TVD Runge-Kutta time discretization

Finally, the semi-discrete scheme must also be discretized in time. We use the third-order TVD Runge-Kutta method (Shu and Osher, 1988; Shu, 1998), which can maintain the stability of the spatial discretization. If we denote the right-hand side of the ordinary differential

equation system by $L(\rho)_{i,j}$, then the Runge-Kutta method is given by

$$\begin{aligned}
\rho^{(1)} &= \rho^n + \Delta t L(\rho^n), \\
\rho^{(2)} &= \frac{3}{4}\rho^n + \frac{1}{4}(\rho^{(1)} + \Delta t L(\rho^{(1)}), \\
\rho^{n+1} &= \frac{1}{3}\rho^n + \frac{1}{4}(\rho^{(2)} + \Delta t L(\rho^{(2)}).
\end{aligned} \tag{45}$$

Here, the time step Δt needs to satisfy the Courant-Friedrichs-Lewy (CFL) condition.

3.5 Solution procedure

We now summarize the complete solution procedure.

Part 1

Starting from the density ρ^n and concentration C^n at time level $t^{1,n}$, we obtain the density ρ^{n+1} and concentration C^{n+1} through the following steps.

1. Obtain the cost function c by the formula (4).
2. Solve the eikonal equation (8) by using the fast sweeping method to obtain ϕ and $\nabla\phi$.
3. Obtain the flux $\boldsymbol{F}$ by using formulas (1), (2), and (7) and the acceleration by formulas (21) and (22).
4. Use the fifth-order Lax-Friedrichs WENO scheme with the third-order TVD Runge-Kutta time discretization to obtain ρ^{n+1} by solving the conservation law.
5. Obtain the source term and solve the advection-diffusion equation to obtain C^{n+1}.

The procedure repeats until it marches to the end of the analysis period.

Part 2

The traffic model and the dispersion model are closely interconnected. When computing the concentration C by solving the advection-diffusion equation, we need to know the density ρ, but they have different initial times, so the solution procedure is different from that in **Part 1**.

Define the vectors of time and the numerical solution at each grid point and each time level as

$$\vec{t} = \{t^{2,n}, n = 1, ..., N_t^2\}. \tag{46}$$

$$\vec{s} = \{s_{i,j}^n = \rho_{i,j}^n E_{i,j}^n,\ i = 1, ..., N_x, j = 1, ..., N_y, n = 1, ..., N_t^2\}. \tag{47}$$

where N_x, N_y and N_t are the numbers of grid points in x, y and t, respectively. The solution procedure is as follows

1. Compute $\vec{t}$ and $\vec{s}$ from $t = t_{end}^2$ to $t = t_{beginning}^2$ by solving the traffic model, using steps 1-3 in the procedure of **Part 1**.

2. Using the values of $\vec{t}$ and $\vec{s}$ to compute the concentration C from $t = t_{beginning}^2$ to $t = t_{end}^2$ by solving the advection-diffusion equation.

4 Numerical experiments

In this section, we first provide a numerical example with a simplified setup to the whole model which has an exact solution, to demonstrate the accuracy of the high-order scheme. We then model and simulate the dispersion of pollution emitted from vehicles in a hypothetical city with a single CBD in a complete day, and then consider the average pollutant concentration.

4.1 Example 1

We reformulated a numerical example as

$$\begin{cases} \rho_t + \nabla \cdot \boldsymbol{F}(x, y, t) = S_1(x, y, t), \\ \| \nabla\phi(x, y, t) \| = \dfrac{1}{v(\rho)}, \\ \boldsymbol{F} = -\rho v^2(\rho) \nabla\phi(x, y, t), \\ \dfrac{\partial C}{\partial t} + \dfrac{\partial (uC)}{\partial x} = \dfrac{\partial}{\partial y}(K_y \dfrac{\partial C}{\partial y}) + \dfrac{\partial}{\partial z}(K_z \dfrac{\partial C}{\partial z}) + S_2(\rho) + S_3. \end{cases} \tag{48}$$

where S_1, S_2 and S_3 are the source terms, chosen so that an explicit exact solution is available, and $v(\rho) = v_0 \exp(-\alpha\rho^2)$.

We solve the system on a domain of $\bar{\Omega} = \Omega \times [0, 2]$, where $\Omega = [-2, 0] \times [-1, 1]$, subject to the following initial and boundary conditions:

$$\begin{aligned} \boldsymbol{F}(x, y, t) \cdot \boldsymbol{n}(x, y) &= q(x, y, t), \quad \forall (x, y) \in \Gamma_o, \\ \rho(x, y, 0) &= \rho_0(x, y), \quad \forall (x, y) \in \Omega, \\ \phi(x, y, t) &= 0, \quad \forall (x, y) \in \Gamma_c. \end{aligned}$$

with the inlet segment $\Gamma_o = \{-2\} \times [-1, 1]$, and the outlet segment $\Gamma_c = \{0\} \times [-1, 1]$.

We denote

$$\begin{aligned} b_1 &= 3e^{-r \sin t}, \\ b_2 &= 12 - 3y + y^3, \\ b_3 &= 9x^2(1 - y^2)^2, \\ v_{log} &= \log[\frac{b_1}{c_f v_0 \sqrt{b_3 + b_2^2}}]. \end{aligned}$$

where r, c_f, v_0, α are given parameters, to write the exact solution as

$$\begin{aligned} \phi_e(x, y, t) &= c_f e^{r \sin t} x(-4 + y - \frac{y^3}{3}), \\ \rho_e(x, y, t) &= \sqrt{-\frac{v_{log}}{\alpha}}, \\ C_e(x, y, z, t) &= \exp -\frac{(x - ut)^2 + y^2 + z^2}{10}, \\ f_{1e}(x, y, t) &= \frac{b_1 b_2 \rho_e}{c_f(b_3 + b_2^2)}, \\ f_{2e}(x, y, t) &= \frac{3b_1 x(-1 + y^2)\rho_e}{c_f(b_3 + b_2^2)}. \end{aligned}$$

with the source terms given by

$$\begin{aligned} S_1(x, y, t) &= \frac{r \cos t}{2\alpha\rho_e}, \\ S_2(\rho, x, y, z) &= \rho_e \exp(-\frac{z^2}{10}), \\ S_3(x, y, z, t) &= (K_y(2 - 4y^2) + K_z(2 - 4z^2)) \exp(-\frac{(x - ut)^2 + y^2 + z^2}{10}) - S_2(\rho). \end{aligned}$$

where

$$
\begin{aligned}
r_1 &= \frac{9b_1x(1-y^2)b_2(1+4v_{log})}{2c_f\alpha(b_3+b_2^2)^2\rho_e},\\
r_{21} &= 3(1-y^2)^2(b_2+6x^2y),\\
r_{22} &= 4(36+9(-17+x^2)y-6(-2+3x^2)y^3+12y^4+9(-1+x^2)y^5+2y^7)v_{log},\\
r_2 &= \frac{3b_1x(r_{21}+r_{22})}{2c_f\alpha(b_3+b_2^2)^2\rho_e}.
\end{aligned}
$$

and the initial and boundary conditions are

$$
q(-2,y,t) = f_{1e}(-2,y,t),\ \ \rho_0(x,y) = \rho_e(x,y,0),\ \ C_0(x,y,z) = C_e(x,y,z,0).
$$

We take the parameters to be $r = 0.01, c_f = 80, v_0 = 1.034, \alpha = 0.01$, and we use high order extrapolation to obtain the values of ghost points at the numerical boundary. We set the exact solution values on the physical boundary, such as Γ_o and Γ_c. The errors and orders of accuracy are shown in Table 2. We can clearly see that the designed order of accuracy is achieved.

Table 2: Errors and orders of accuracy for the density ρ, potential ϕ and concentration C

N	L^2 error of ρ	order	L^2 error of ϕ	order	L^2 error of C	order
10	7.11E-06	–	1.67E-01	–	4.23E-07	–
20	1.68E-07	5.40	2.36E-02	2.83	1.09E-08	5.27
40	2.50E-09	6.07	3.27E-03	2.85	3.24E-10	5.11
80	3.17E-11	6.30	4.34E-04	2.91	8.96E-12	5.19
160	3.85E-13	6.36	4.85E-05	3.16	2.49E-13	5.18

4.2 Example 2

4.2.1 Problem description

As shown in Figure 2, we consider a rectangular domain 35 km long and 25 km wide in the numerical simulation. The center of the compact CBD is located at (10 km, 10 km) with a diameter of 2 km, and a lake is located at (25 km, 15 km) with a diameter of 2 km, and we simulate the pollution dispersion in three dimensions 1 km above the rectangular domain (i.e., $\Omega = [0,35] \times [0,25]$, $\bar{\Omega} = \Omega \times [0,1]$). We assume that there is no traffic at the beginning of

the modeling period (i.e., $\rho_0(x, y) = 0,\ \forall (x, y) \in \Omega$), and that no cost is incurred by entering and leaving the CBD ($\phi_{CBD} = 0,\ \forall (x, y) \in \Gamma_c,\ t \in T$). We consider the dispersion from 6:00 am to 6:00 am the following day in the city, so the modeling period is $T = [0, 24h]$. We set $T^1 = [0, 11h]$, $T^2 = [11, 24h]$. The traffic demand function q is defined as

$$q(x, y, t) = q_{max}[1 - \gamma_1 d(x, y)]g(t). \tag{49}$$

where $q_{max} = 240\ veh/km^2/h$ is the maximum demand, $d(x, y) = \sqrt{(x - 10)^2 + (y - 10)^2}$ is the distance from the location (x, y) to the center of the CBD, and $\gamma_1 = 0.01\ km^{-1}$. The factor $[1 - \gamma_1 d(x, y)]$ is used to express the higher traffic demand generated in the domain closer to the CBD, where more of the population is located, and finally, $g(t)$ is a time-varying function defined by

$$g(t) = \begin{cases} t, & t \in [0, 1h], \\ 1, & t \in [1, 2h], \\ -\frac{4}{5}(t - 2) + 1, & t \in [2, 3h], \\ 0.2 & t \in [3, 5h], \\ 0, & t \in [5, 12h], \\ -t + 12, & t \in [12, 13h], \\ -1, & t \in [13, 14h], \\ \frac{4}{5}(t - 14) - 1, & t \in [14, 15h], \\ -0.2, & t \in [15, 17h], \\ 0, & t \in [17, 24h]. \end{cases} \tag{50}$$

The speed function is defined as $U(x, y, t) = U_f e^{-\beta\rho^2}$, in which $\beta = 2 \times 10^{-6}\ km^4/veh^2$ and $U_f(x, y)$ is the free-flow speed given by

$$U_f(x, y) = U_{max}[1 + \gamma_2 d(x, y)]. \tag{51}$$

where $U_{max} = 56\ km/h$ is the maximum speed and $\gamma_2 = 4 \times 10^{-3}\ km^{-1}$. The factor $[1 + \gamma_2 d(x, y)]$ is used to express the faster free-flow speed in the domain far from the CBD, where there are

fewer junctions. The local travel cost per unit of distance is defined as $c(x, y, t) = \kappa(\frac{1}{U} + \pi(\rho))$, where $\kappa = 90\ \$/h$ and $\pi(\rho) = 10^{-8}\rho^2$, We assume that the capacity of the CBD is large enough to accommodate all of the travelers in the city, so $|\boldsymbol{F}|$ should maintain the maximum flow intensity at the CBD boundary under the congested condition. We assume the wind velocity is constant, and $|\boldsymbol{u}_f| = 5\ km/h,\ 10km/h$ is used for next consideration, and $K_x = K_y = K_z = 0.01\ km^2/h$.

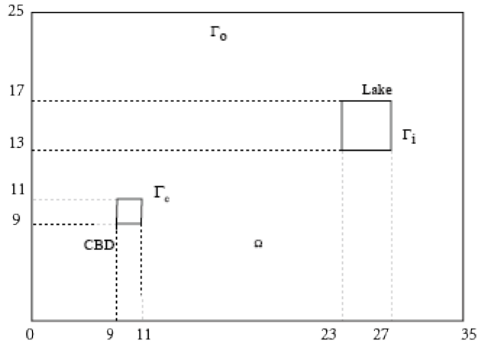

Fig. 2: The modeling domain

In this study, we consider the dispersion of the vehicle exhaust in the city under these eight different wind directions, they are west, south, east, north, southwest, southeast, northeast and northwest directions respectively. Next, we introduce the boundary condition for the dispersion model under different wind directions. For the west wind: $C(35, y, z, t) = 0$, the term $K_x\partial_x^2 C$ is neglected; for the east wind: $C(0, y, z, t) = 0$, the term $K_x\partial_x^2 C$ is neglected; for the south wind: $C(x, 25, z, t) = 0$, the term $K_y\partial_y^2 C$ is neglected; for the north wind: $C(x, 0, z, t) = 0$, the term $K_y\partial_y^2 C$ is neglected; for the northeast wind: $C(0, y, z, t) = 0, C(x, 0, z, t) = 0$, the terms $K_x\partial_x^2 C$ and $K_y\partial_y^2 C$ are neglected; for the northwest wind: $C(35, y, z, t) = 0, C(x, 0, z, t) = 0$, the terms $K_x\partial_x^2 C$ and $K_y\partial_y^2 C$ are neglected; for the southeast wind: $C(0, y, z, t) = 0, C(x, 25, z, t) = 0$, the terms $K_x\partial_x^2 C$ and $K_y\partial_y^2 C$ are neglected; for the southwest wind: $C(35, y, z, t) = 0$, $C(x, 25, z, t) = 0$, the terms $K_x\partial_x^2 C$ and $K_y\partial_y^2 C$ are neglected.

We now use the algorithm described in the previous section to perform the numerical simulation. A mesh with a $N_x \times N_y \times N_z$ grid is used. The numerical boundary conditions are summarized as follows.

1. On the solid wall boundary, i.e., the outer boundary of the city, Γ_o, and the boundary of the obstruction, Γ_i, we let the normal numerical flux be 0. We set $\rho = 0$ at the ghost points inside the wall. In the Eikonal equation, we set $\phi = 10^{12}$ at the ghost points.

2. On the boundary of the CBD, i.e., Γ_c, we set $\phi = 0$ in the eikonal equation. The boundary conditions for ρ inside the CBD are obtained by extrapolation from the grids outside the CBD. To maintain the maximum flow intensity on the boundary of the CBD under the congested condition, we set $U(x, y, t) = U_f$ inside the CBD.

4.2.2 Numerical results

We present the numerical results in this subsection. To verify the convergence of the algorithm with grid refinements, we simulate using two meshes with $140 \times 100 \times 150$ and $280 \times 200 \times 300$ grid points, respectively. The density curves and concentration curves at 8:00 am along different cuts are plotted in Figure 3, and show good grid convergence for the numerical solution. The grid $140 \times 100 \times 150$ is selected for further discussion

Figure 4 shows the temporal and spatial distributions of the density ρ within the modeling region. As shown in Figure 4(a), the density is low at the beginning and the traffic is in the non-congested condition. As the traffic demand grows, more vehicles gradually join the traffic system, the region near the CBD boundary becomes congested, and the density in the eastern region is particularly high (see Figure 4(b)). Although the demand starts to decrease from 8:00 am, the areas around the CBD are still in the congested condition at 8:30 am due to the limitation on the maximum flow intensity into the CBD (Figure 4(d)). As the demand decreases further, all parts of the city return to the non-congested condition (Figure 4(e) and (f)). Then, because the traffic demand becomes zero and all the travelers have entered the CBD, there is no traffic in the city until the vehicles return from the CBD. As the vehicles begin to return from the CBD the density increases (Figure 4(g) and (h)), and although the traffic demand starts to decrease from 7:00 pm, the density keeps increasing due to the flow intensity being greater than the traffic demand (Figure 4(i)). As the demand decreases further,

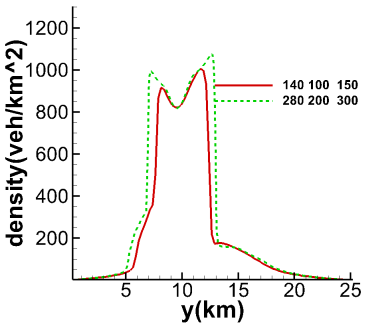

(a) x=12

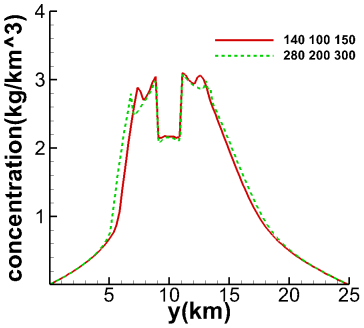

(b) x=12

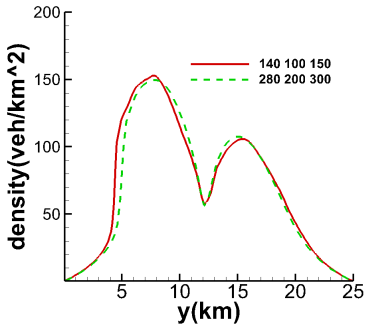

(c) x=16

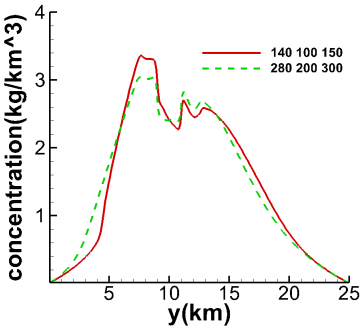

(d) x=16

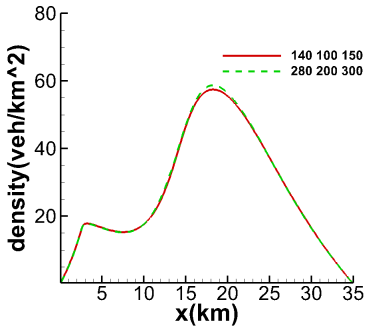

(e) y=3

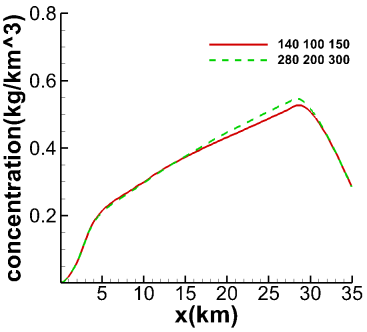

(f) y=3

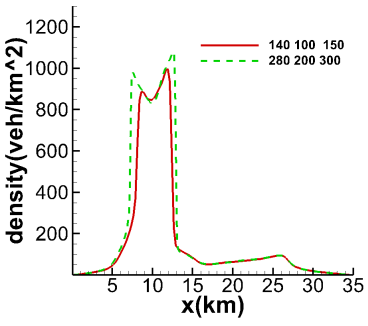

(g) y=12

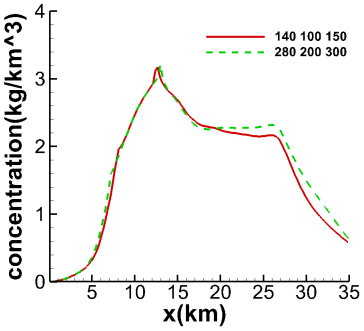

(h) y=12

Fig. 3: Demonstration of grid convergence of the density(unit: veh/km^2) (left column, panels a, c, e, g) and of the concentration(unit: kg/km^3) (right column, panels b, d, f, h) at 8:00 am

the city returns to the non-congested condition (Figure 4(j), (k) and (l)). Finally, all vehicles have reached their destinations, and there is no traffic in the city.

Figure 5 illustrates the contours of the total cost potential function ϕ at various times. At the beginning of the modeling period, when the density is very low and traffic is in a free-flow state, the cost potential contours are a series of concentric circles located around the CBD. As the traffic demand grows, the total cost potential increases and the contours become denser. As the spaces between the contours become smaller, the local cost of moving one distance unit increases, as shown in Figure 5(b). In Figure 5(c) and (d), the density on the eastern side of the CBD is very high and the travel cost increases rapidly, resulting in a denser set of cost potential contours in this region. As the traffic demand decreases, the distributions of the cost potential function return to their former conditions, as shown in Figure 5(e) and (f). The density initially increases and the contours become denser again when the vehicles return from CBD (Figure 5(h) and (i)). As the vehicles gradually reach their homes, the cost potential contours return to being a series of concentric circles located around the CBD (Figure 5(l)).

Figure 6 shows the plot of the flow vector, which illustrates the results of the path choice. We can see that the travelers pass around the lake if they come from the east. At the beginning and end of the two modeling period, as the density is low, vehicles move toward the CBD or leave CBD in almost straight lines. As the density of the eastern region around the CBD becomes high, vehicles choose a curved trajectory to avoid this region. This demonstrates the capability of the proposed RDUO-C model in modeling how travelers alter their preferred routes in response to dynamic changes in the network conditions to minimize their instantaneous cost potentials.

We consider the total flow to the CBD through Γ_c (consisting of the inflow when the vehicles travel to the CBD and the outflow when the vehicles return from the CBD; if $f_{CBD} > 0$, it represents the inflow, otherwise, it represents the outflow) defined as

$$f_{CBD}(t) = \oint_{\Gamma_c} (\boldsymbol{F} \cdot \boldsymbol{n})(x, y, t) ds. \tag{52}$$

where $\boldsymbol{n}$ is the unit normal vector pointing toward the CBD, and the total demand over the

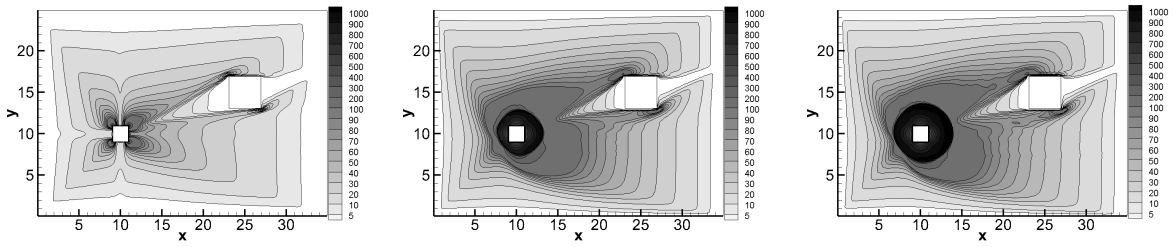

(a) 6:30 am (b) 7:30 am (c) 8:00 am

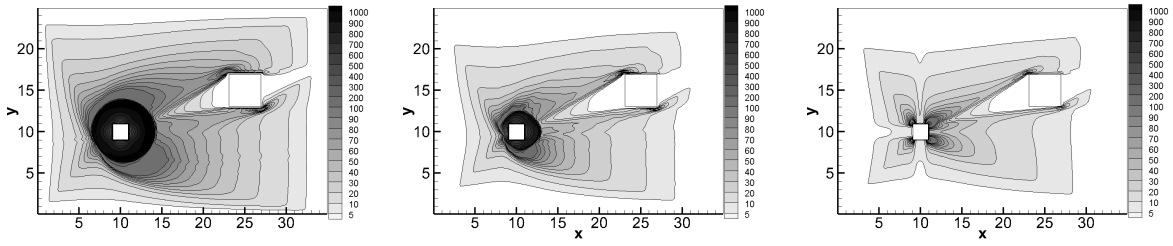

(d) 8:30 am (e) 9:00 am (f) 11:00 am

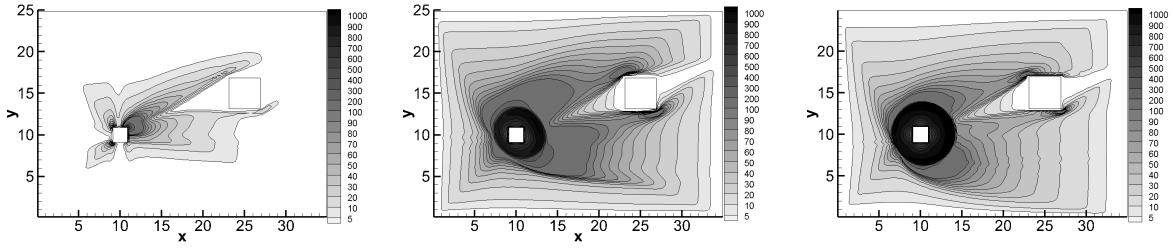

(g) 6:00 pm (h) 7:00 pm (i) 7:30 pm

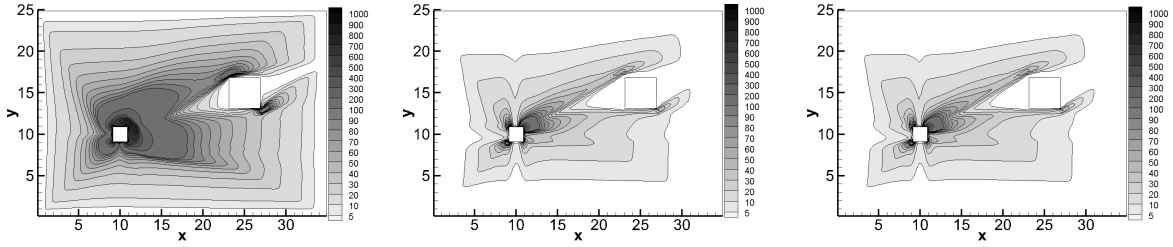

(j) 8:00 pm (k) 9:00 pm (l) 10:30 pm

Fig. 4: Density plot(unit: veh/km^2)

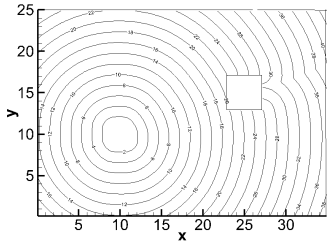

(a) 6:30 am

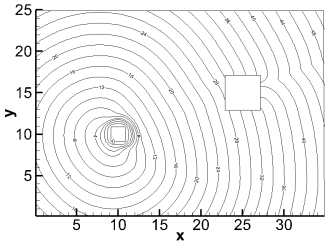

(b) 7:30 am

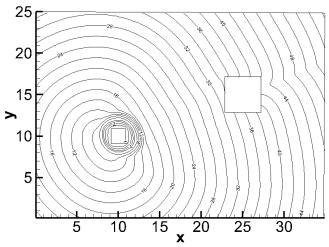

(c) 8:00 am

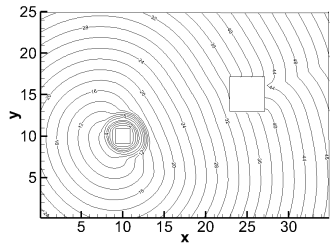

(d) 8:30 am

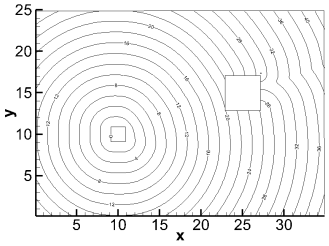

(e) 9:00 am

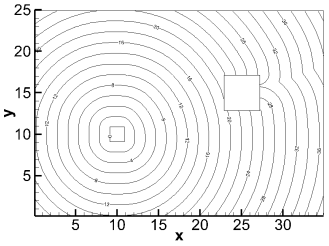

(f) 11:00 am

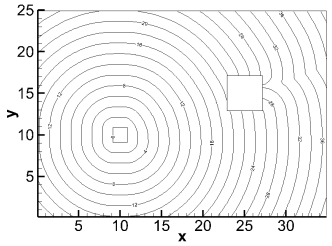

(g) 6:00 pm

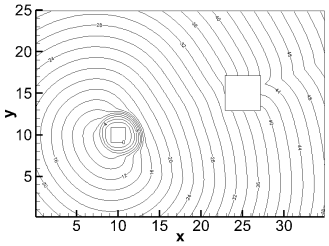

(h) 7:00 pm

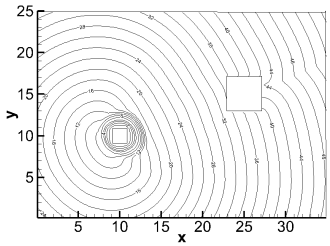

(i) 7:30 pm

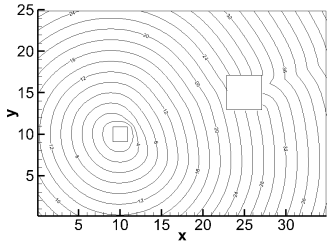

(j) 8:00 pm

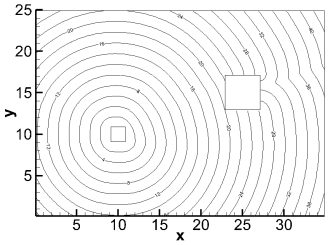

(k) 9:00 pm

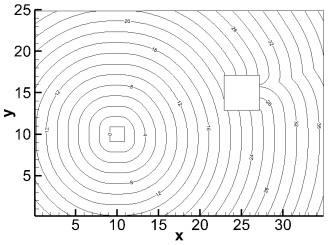

(l) 10:30 pm

Fig. 5: Cost potential plot

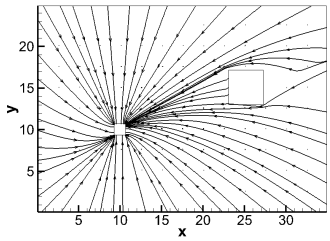

(a) 6:30 am

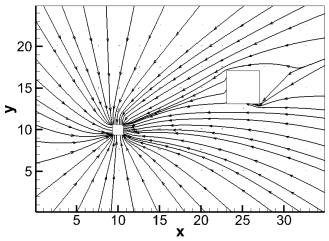

(b) 7:00 am

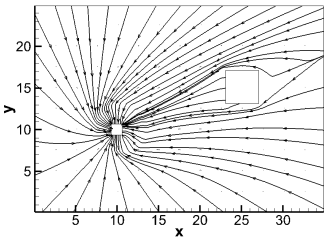

(c) 8:00 am

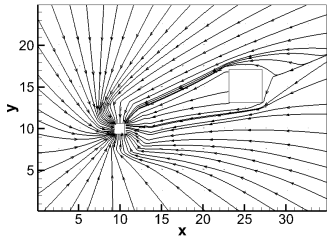

(d) 8:30 am

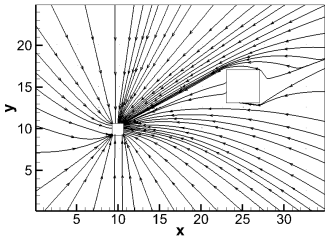

(e) 9:00 am

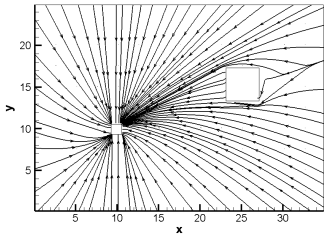

(f) 11:00 am

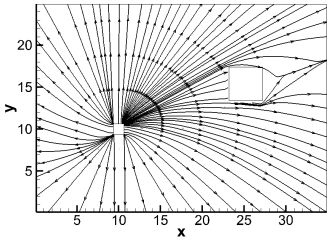

(g) 6:00 pm

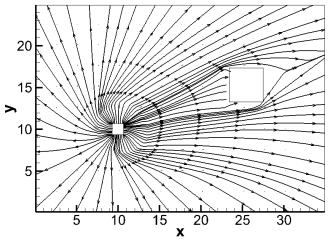

(h) 7:00 pm

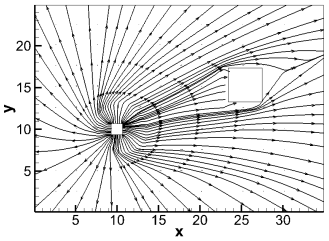

(i) 7:30 pm

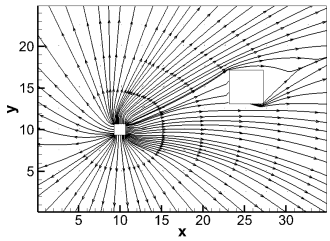

(j) 8:00 pm

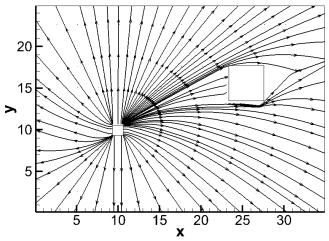

(k) 9:00 pm

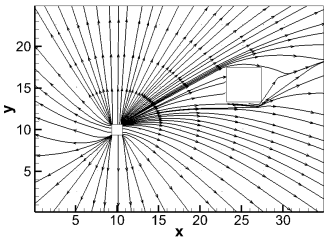

(l) 10:30 pm

Fig. 6: Flow vector plot

whole domain is defined as

$$q_\Omega(t) = \iint_\Omega q(x, y, t)dxdy. \tag{53}$$

Figure 7 shows the relationship between $f_{CBD}(t)$ and $q_\Omega(t)$. The numerical datas show that the areas under these two curves are the same, which demonstrates that all the vehicles have entered the CBD by 11:00 am, and have left the CBD and reached their homes by 11:00 pm. The curve for the total inflow $f_{CBD}(t)$ always lags behind the curve for the total demand $q_\Omega(t)$. In contrast, the curve for the total demand $q_\Omega(t)$ always lags behind the curve for the total outflow $f_{CBD}(t)$. The number of vehicles in the city increases when $q_\Omega(t)$ is larger than $f_{CBD}(t)$, and it decreases when $f_{CBD}(t)$ is larger than $q_\Omega(t)$.

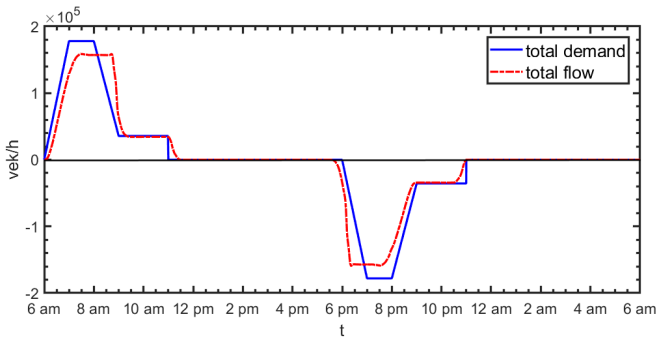

Fig. 7: The total demand and total inflow plot

Figure 8 shows the temporal and spatial distribution of the pollutant concentration C for NO_x at ground level in a complete day, given the wind direction aligned with the positive x-axis and $|\boldsymbol{u}_f| = 10\ km/h$. This figure clearly shows that the upwind locations are much less polluted than the downwind locations, due to the dispersion effect. In addition, comparing the figures reveals a positive relationship between the traffic flow intensity and the pollutant concentration, but the most polluted time always lags behind the most congested time.

Consider the pollutant average concentration at the ground level in a complete day, defined as

$$\bar{C}(x, y) = \frac{1}{24}\int_0^{24} C(x, y, 0, t)dt. \tag{54}$$

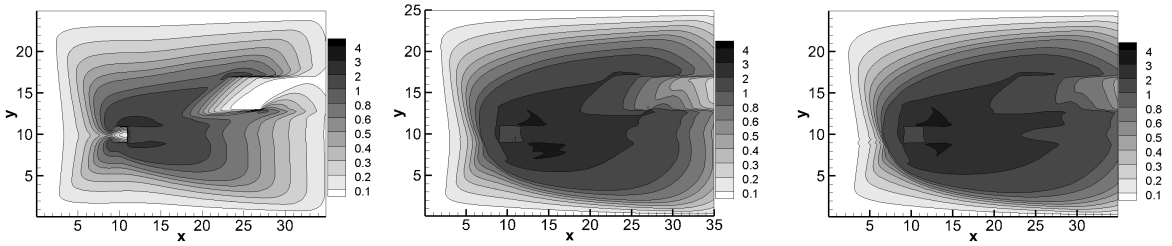

(a) 7:00 am (b) 8:00 am (c) 8:30 am

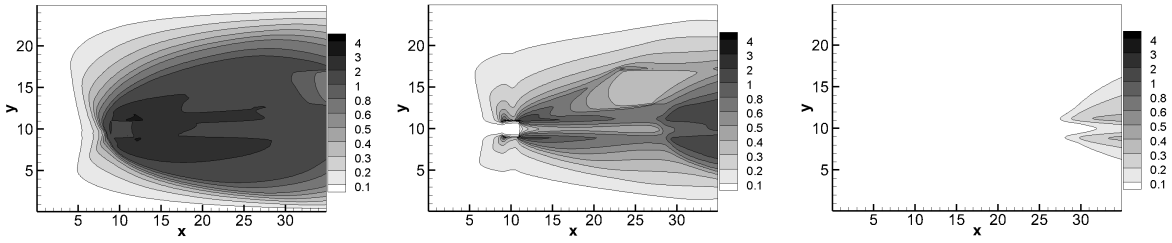

(d) 9:00 am (e) 11:00 am (f) 1:00 pm

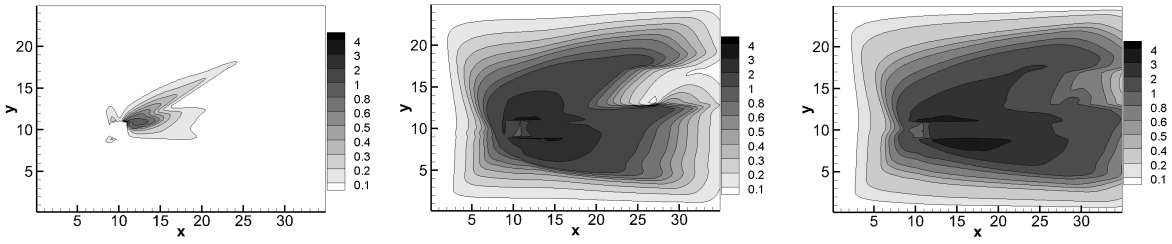

(g) 6:00 pm (h) 7:00 pm (i) 8:00 pm

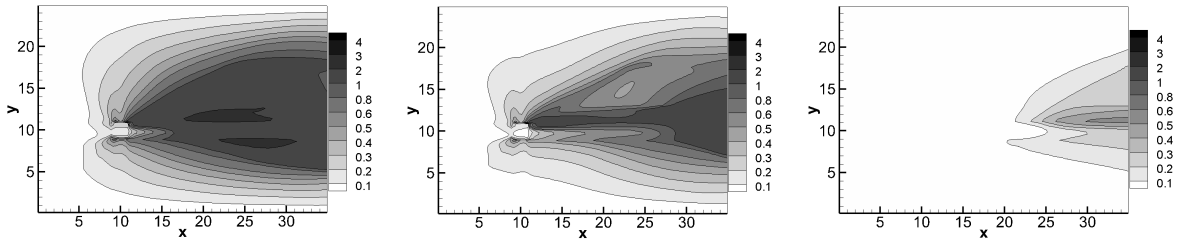

(j) 9:00 pm (k) 10:00 pm (l) 12:00 am

Fig. 8: Concentration plot (unit: kg/km^3)

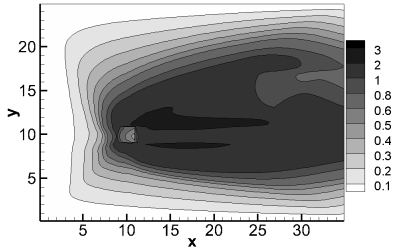

(a) west

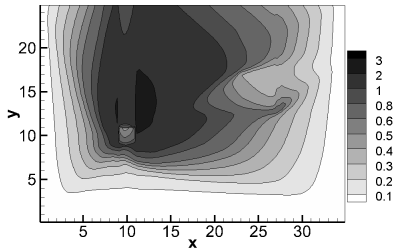

(b) south

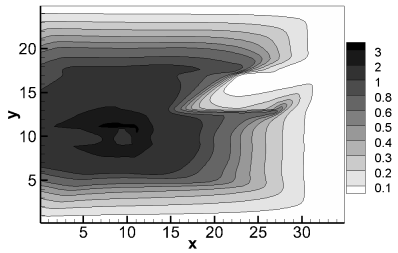

(c) east

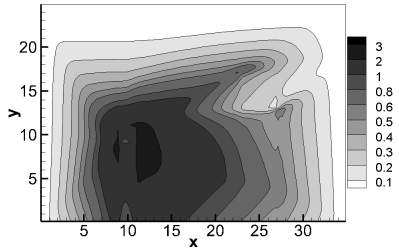

(d) north

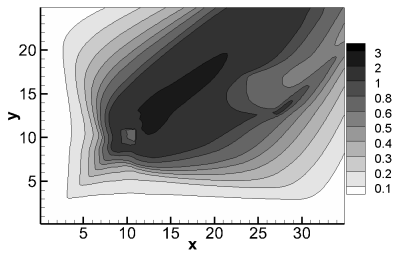

(e) southwest

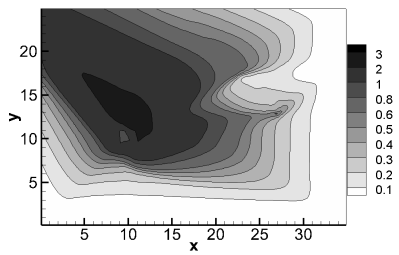

(f) southeast

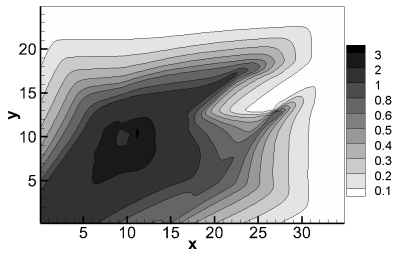

(g) northeast

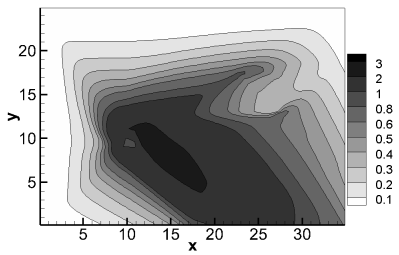

(h) northwest

Fig. 9: An average concentration plot for a day under different wind directions, and $\boldsymbol{u_f}$ = 10 km/h (unit: kg/km^3)

Figure 9 shows the distribution of the pollutant average concentration $\bar{C}$ under different wind directions over the city region. The sub-figures in Figure 9 show the results with the wind direction aligned with west, south, east, north, southwest, southeast, northeast and northwest directions respectively. As shown in the figure, the high-pollution areas are mainly located at the downwind location around the CBD, and the northeast region is always highly polluted due to the high density of vehicles.

Same as the daily average concentration $\bar{C}$, we can also define the pollutant average concentration in a year according to the type of wind. Typically, the wind direction is the same at the same time in a year for a fixed city. We assume that the distribution of wind is the same every year, including the velocity, direction, and the period for each type of wind. We can then define

$$\tilde{C}(x, y) = \sum_{i=1}^{N} k_i \bar{C}_i(x, y). \tag{55}$$

where N is the amounts of the type of wind, and $\bar{C}_i$ is the pollutant average concentration of a day with the wind introduced as above, and k_i is the corresponding weight, and satisfying $\sum_{i=1}^{N} k_i = 1$.

Figure 10 shows the wind rose plot of the different distributions of wind in a year. The wind velocity is 5 km/h and 10 km/h, and the wind direction is one of the eight directions as mentioned, so $N = 16$, for simplicity to describe, we numbered all winds that consideration in the study as in Table 3

Table 3: The number of each type wind

number	north	northeast	east	southeast	south	southwest	west	northwest
5km/h	1	3	5	7	9	11	13	15
10km/h	2	4	6	8	10	12	14	16

Figure 11 show the distribution of $\tilde{C}$ within the modeling region according to the distribution of wind in the Figure 10. These figures show that the highly polluted region is located around the CBD and particularly in the northeast region, and different weights have an obvious

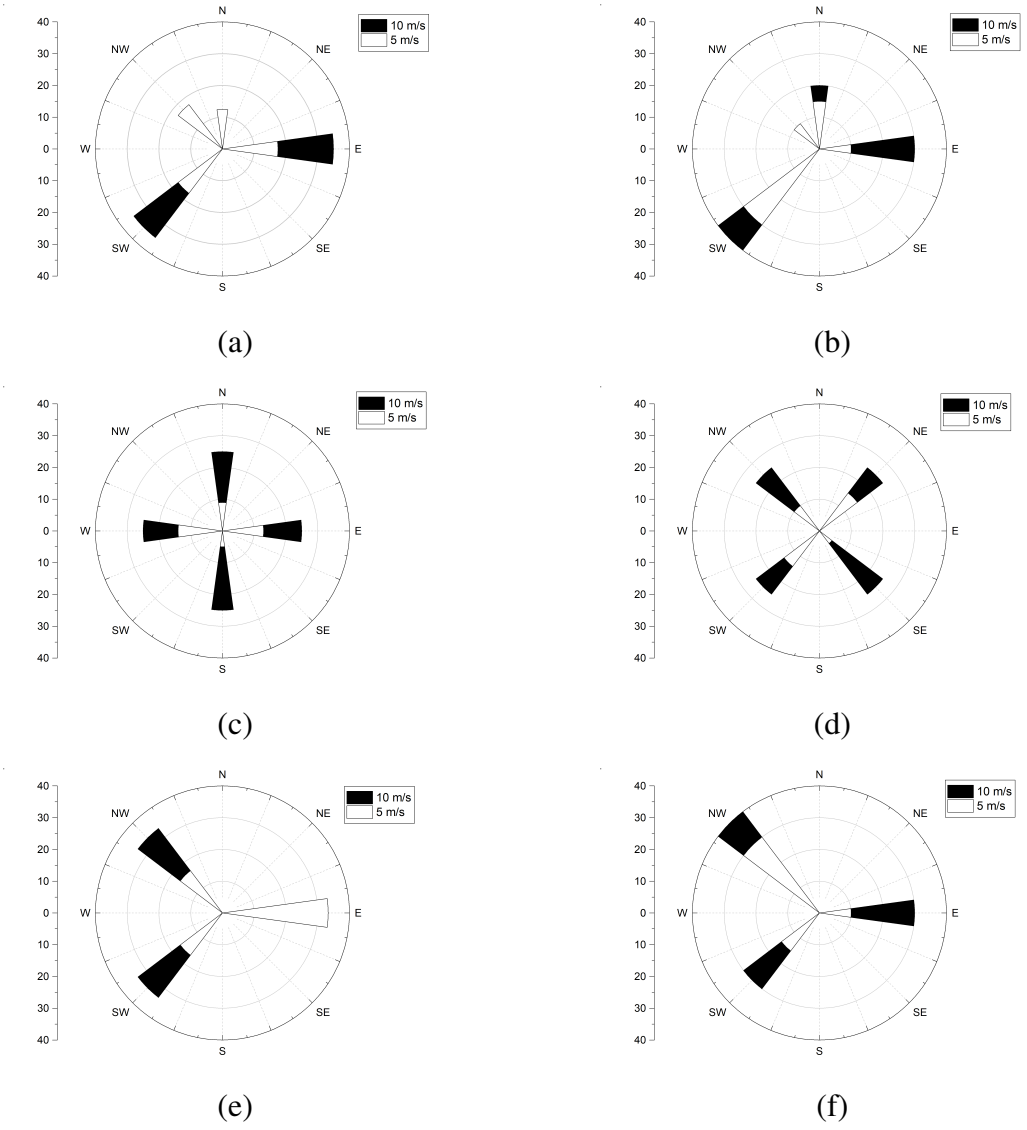

Fig. 10: Wind rose plot of the distribution of wind (the weights under each type wind in the sub-figures are: (a) k_1=0.125, $k_5 = k_6 = k_{11} = k_{12} = k_{15}$=0.175, (b) k_1=0.16, k_2=0.04, $k_5 = k_{15} = k_{12}$=0.1, k_6=0.2, k_{11}=0.3, (c) k_1=0.09, k_2=0.16, k_5=0.13, k_6=0.12, k_9=0.05, k_{10}=0.2, k_{13}=0.14, k_{14}=0.11, (d) $k_3 = k_{16}$=0.15, $k_4 = k_{15}$=0.10, k_7=0.05, k_8=0.20, k_{11}=0.14, k_{12}=0.11, (e) k_5=1/3, $k_{11} = k_{12} = k_{15} = k_{16}$=1/6, (f) $k_5 = k_{16}$=0.1, k_6=0.2, $k_{11} = k_{12}$=0.15, k_{15}=0.3, where $i = 1, 2, ..., 16$ is the number of the wind in Table 3)

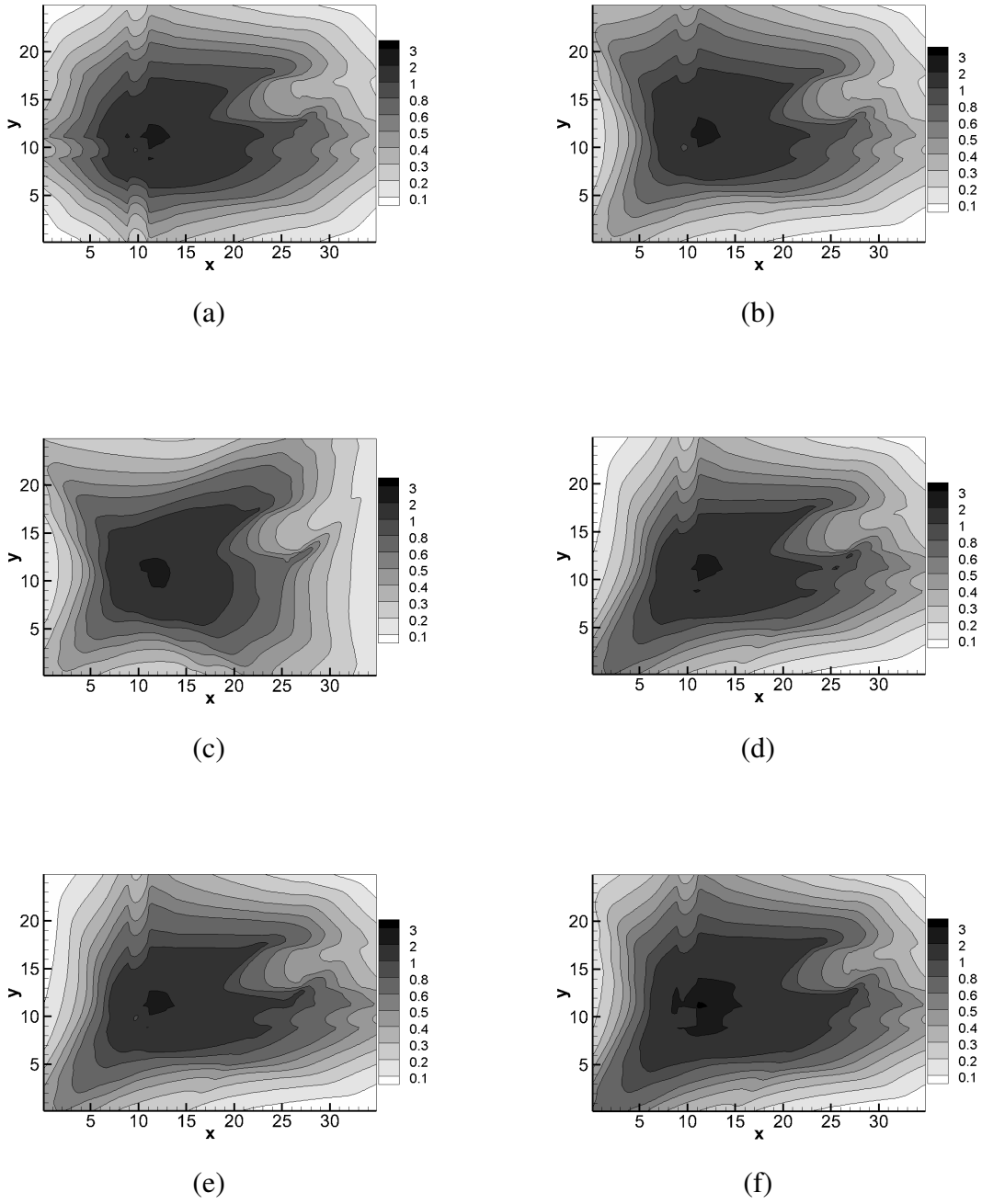

Fig. 11: Average concentration plots for 1 year (the weights under each type wind in the sub-figures are: (a) k_1=0.125, $k_5 = k_6 = k_{11} = k_{12} = k_{15}$=0.175, (b) k_1=0.16, k_2=0.04, $k_5 = k_{15} = k_{12}$=0.1, k_6=0.2, k_{11}=0.3, (c) k_1=0.09, k_2=0.16, k_5=0.13, k_6=0.12, k_9=0.05, k_{10}=0.2, k_{13}=0.14, k_{14}=0.11, (d) $k_3 = k_{16}$=0.15, $k_4 = k_{15}$=0.10, k_7=0.05, k_8=0.20, k_{11}=0.14, k_{12}=0.11, (e) k_5=1/3, $k_{11} = k_{12} = k_{15} = k_{16}$=1/6, (f) $k_5 = k_{16}$=0.1, k_6=0.2, $k_{11} = k_{12}$=0.15, k_{15}=0.3, where $i = 1, 2, ..., 16$ is the number of the wind in Table 3)(unit: kg/km^3)

influence on the distribution of $\tilde{C}$, so it is important to take into account the wind distribution when selecting the location of the CBD.

5 Conclusion

In this study, the continuum modeling approach is taken to study the dispersion of vehicle exhaust in a city. We first used the model in Huang et al. (2009) to describe the traffic flow that satisfies the reactive dynamic user equilibrium principle in which a vehicle chooses a route to minimize the instantaneous travel cost to the destination. We have demonstrated that the problem of vehicles returning from the CBD is simply a reversal of the problem of vehicles traveling to the CBD. We then consider the dispersion of vehicle exhaust due to the turbulent eddy motion and wind. The concentration of the pollutant is governed by an advection-diffusion equation with a Dirac source term. We have described an efficient solution algorithm for the complete model, including the weighted essentially non-oscillatory (WENO) finite difference scheme for the conservation equation, the fast sweeping method with WENO approximation for the eikonal equation, a regularized function is used to approximate the Dirac function, and fifth-order WENO approximation to the advection term in the advection-diffusion equation. The numerical results show a reasonable temporal and spatial distribution of the vehicle density and the pollution concentration.

The formulation in this paper only applies to a region with a single CBD. We can extend our model to the case of multiple CBDs, for which the flows would interact in the city, and thus the model would become more complicated. This would make for an interesting future study. We can also consider how the air quality affects the choice of residential locations, which in turn changes travel behavior and hence the pollution patterns. An optimal housing distribution could then be achieved.

Acknowledgements

The work described in this paper was supported by a grant from the Research Grants Council of the Hong Kong Special Administrative Region, China (Project No. 17208614). The third author was also supported by the Francis S Y Bong Professorship in Engineering. The research of the fourth author is supported by ARO grant W911NF-15-1-0226 and NSF grant DMS-1719410. The research of the fifth author is supported by NSFC Grant 11471305.

References

Ahn, K., Trani, A.A., Rakha, H. and van Aerde, M. (1999) Microscopic fuel consumption and emission models. Transportation Research Board 78th Annual Meeting, Washington DC.

Arya, S.P. (1999) Air Pollution Meteorology and Dispersion. Oxford University Press, New York.

Crandall M. and Lions P.L. (1983) Viscosity solutions of Hamilton-Jacobi equations. Transactions of American Mathematical Society, 277, 1-42.

Ermak, D.L. (1977) An analytical model for air pollutant transport and deposition from a point source. Atmospheric Environment, 11(3): 231-237.

Huang, L., Wong, S.C., Zhang, M.P., Shu, C.W., and Lam, W.H.K. (2009) Revisiting Hughes' dynamic continuum model for pedestrian flow and the development of an efficient solution algorithm. Transportation Research Part B, 43(1): 127-141.

Jiang G. and Shu C.-W. (1996) Efficient implementation of weighted ENO schemes. Journal of Computational Physics, 126, 202-228.

Jiang G. and Peng D.P. (2000) Weighted ENO schemes for Hamilton-Jacobi equations. SIAM Journal on Scientific Computing, 21, 2126-2143.

Liu X.D., Osher S. and Chan T. (1994) Weighted essentially nonoscillatory schemes. Journal of Computational Physics, 115(1), 200-212.

Lushi, E. and Stockie, J.M. (2010) An inverse Gaussian plume approach for estimating atmospheric pollutant emissions from multiple point sources. Atmospheric Environment, 44(8): 1097-1107.

Nagendra, S.M.S. and Khare, M. (2002) Line source emission modelling. Atmospheric Environment, 36(13): 2083-2098.

Pasquill, F. (1961) The estimation of dispersion of windborne material. Meteorol. Mag., 90: 22-49.

Roberts, O.F.T. (1923) The theoretical scattering of smoke in a turbulent atmosphere. Proceedings of the Royal Society of London. Series A, 104(728): 640-654.

Shu C.-W. (1998) Essentially non-oscillatory and weighted essentially non-oscillatory schemes for hyperbolic conservation laws. In Advanced Numerical Approximation of Nonlinear Hyperbolic Equations, B. Cockburn, C. Johnson, C.-W. Shu and E. Tadmor (Editor: A. Quarteroni), Lecture Notes in Mathematics, volume 1697, Springer, Berlin, 325-432.

Shu C.-W. (2007) High order numerical methods for time dependent Hamilton-Jacobi equations, in Mathematics and Computation in Imaging Science and Information Processing, S.S. Goh, A. Ron and Z. Shen, Editors, Lecture Notes Series, Institute for Mathematical Sciences, National University of Singapore, volume 11, World Scientific Press, Singapore, 47-91.

Shu C.-W. and Osher S. (1988) Efficient implementation of essentially non-oscillatory shock capturing schemes. Journal of Computational Physics, 77, 439-471.

Stockie, J.M. (2011) The mathematics of atmospheric dispersion modeling. SIAM Review, 53(2): 349-372.

Sutton, O.G. (1932) A theory of eddy diffusion in the atmosphere. Proceedings of the Royal Society of London. Series A, 135(826): 143-165.

Tornberg A.K. and Engquist B. (2004) Numerical approximations of singular source terms in differential equations. Journal of Computational Physics, 200(2): 462-488.

Wardman, M. and Bristow, A.L. (2004). Traffic related noise and air quality valuations: Evidence from stated preference residential choice models. Transportation Research Part D: Transport and Environment, 9, 1-27.

Whaley, H. (1974) The derivation of plume dispersion parameters from measured three-dimension data. Atmospheric Environment, 8: 281-290.

Wikipedia(2010). Inversion (meteorology) Source: *http* : *//en.wikipedia.org/wiki/Inversion_(meteorology)*. Accessed 23 March 2010

Yin J., Wong S.C., Sze N.N. and Ho H.W. (2013) A continuum model for housing allocation and transportation emission problems in apolycentric city. International Journal of Sustainabe Transportation, 7, 275-298.

Yin J., Wong S.C., Choi K. and Du Y.C. (2017) A continuum modeling approach to the spatial analysis of air quality and housing location choice. International Journal of Sustainabe Transportation, 11, 319-329.

Xiong, T., Zhang, M., Shu, C.-W., Wong, S.C. and Zhang, P. (2011) High-order computational scheme for a dynamic continuum model for bi-directional pedestrian flows. Computer-Aided Civil and Infrastructure Engineering, 26, 298-310.

Zhang Y.T., Zhao H.K. and Qian J. (2006) High order fast sweeping methods for static Hamilton-Jacobi equations. Journal of Scientific Computing, 29 (1), 25-56.

Zhao, H.K. (2005). A fast sweeping method for Eikonal equations. Mathematics of Computation 74 (250), 603-627.